Control oriented estimation of the exchange current density in PEM fuel cells via stochastic filtering

José Agustín Aguilar [*,a], Juan Andrade-Cetto [a], Attila Husar [a,b]

[a] Institut de Robòtica i Informàtica Industrial, CSIC-UPC

Llorens Artigas 4-6, 08028 Barcelona, Spain.

[b] Dept. Mecànica de Fluids, UPC

Pavelló 1, Diagonal 647, 08028, Barcelona, Spain

Abstract

Increasing efficiency and durability of fuel cells can be achieved through advanced model-based optimal control of its operating conditions, and the efficient online estimation of fuel cell parameters and internal states is fundamental for the implementation of such advanced controllers. The exchange current density is a driving parameter of performance for the catalyst layer of proton exchange membrane fuel cells (PEMFC). This study presents a control oriented, stochastic filtering approach for online, continuous estimation of the exchange current density in low temperature PEMFCs. The fuel cell is framed as a Markov model where the exchange current density is posed as the stochastic hidden state. The physics-based static equation of the exchange current density is converted into a state transition equation. This transition equation and the equation for cell voltage are used in the stochastic state estimator to approximate the posterior probability distribution of the exchange current density. In order to highlight the usefulness of the approach, the estimated value of the exchange current density is used to approximate the trend of the electrochemical active surface area (ECSA) in the catalyst layer and train a nonlinear auto-regressive model. This data-driven model is used to forecast the evolution in the ECSA associated with long term degradation. The estimation algorithm is successfully implemented and tested in two different experimental datasets.

Keywords: PEM fuel cell, exchange current density, particle filter, electrochemical active surface area, state estimation, data-driven model.

*Corresponding author. jaguilar@iri.upc.edu

1 Introduction

Proton exchange membrane fuel cells (PEMFCs) are a promising alternative for replacing hydrocarbon-fueled internal combustion engines in the powertrain of long distance, heavy payload transport vehicles. However, there are a number of issues that must be addressed in order to consider PEMFCs a viable commercial option. Cell durability and efficiency are among the most relevant of these issues. The U.S. Department of Energy, in its last Hydrogen and Fuel Cell Technologies Office Multi-Year Research, Development, and Demonstration Plan, has set a durability target of at least 25,000 hours for fuel cell systems in buses and heavy duty transport applications [1]. This goal is still out of reach for commercially available membrane electrode assemblies.

Several studies have shown that operating conditions have a major influence on fuel cell durability and efficiency. The relation between the operating conditions of the cell such as voltage profile, temperature or relative humidity, and the dissolution of platinum in the catalyst layer has been identified [2]. Other studies have modeled the effect of voltage profile and humidity on the corrosion of the catalyst layer carbon support [3], and analytical expressions for platinum dissolution, platinum oxidation and more chemical degradation mechanisms as a function of cell temperature, humidity and load profile have been established [4]. The degradation of the catalyst layer has been related to the operating conditions in practical applications [5].

Thus, appropriate control of the operating conditions is hence necessary to reach the aforementioned durability goal. Advanced control algorithms rely heavily on the availability of accurate fuel cell models, but these models require the extraction or estimation of a large number of parameters and internal states, which are not easily measurable outside of the laboratory setting or without the use of special instruments. Moreover, these parameters change during fuel cell operation.

Among the most recent algorithms used for fuel cell parameter estimation are bio-inspired optimization algorithms such as hybrid artificial bee colony differential optimizers [6], genetic algorithms [7], manta ray foraging optimizers [8], improved chaotic MayFly optimization [9], hybrid interior search algorithm [10], modified gorilla troop optimizer [11], bi-subgroup optimization [12], adaptive sparrow search [13], chaos embedded particle swarm optimization [14], improved monarch butterfly optimizer [15], water strider algorithm [16]. These bio-inspired optimization algorithms can find the global minimum in the parameter space and are robust in dealing with the non-linearities in the fuel cell model. However, they tend to have large computational burden, making them unfitted for online estimation. Therefore, these approaches are only useful to estimate constant, non-dynamic parameters for off-line fitting of a, physics-based, static fuel cell model. Furthermore, these algorithms assume a perfect knowledge of the physics-based analytical expressions of the fuel cell.

Other deterministic approaches have been used for online, real-time estimation. The objective in this case is to continuously observe dynamically changing parameters or internal states while the fuel

cell is in operation. Some of these studies include high order sliding mode observers for estimating the oxygen concentration in the cathode catalyst layer [17]; adaptive sliding mode observers for estimating the parameters in a semi-empirical fuel cell model to control the oxygen excess ratio [18]; nonlinear dynamic state observers for estimating cell voltage and cell current in sensorless low-cost applications [19], or the profiles of gas species and partial pressures in fuel cells delivery systems [20]. Also, nonlinear parameter observers have been proposed for estimating the electrochemical active surface area (ECSA) in the cathode catalyst layer [21] or the hydrogen partial pressure in the anode channel [22]. The main drawback in all these deterministic algorithms is that they do not take explicitly into account the inherent stochastic nature of the model due to the uncertainty in the rest of parameters and internal states.

On the other hand, there has been also stochastic based approaches to the problem of parameter estimation, for both off-line and online operation. These methods take into account the uncertainty in the fuel cell model. Some studies propose the use of particle filters [23, 24] or extended Kalman filters [25] to estimate the coefficients of an experimentally obtained degradation curve, with the objective of predicting the remaining useful lifetime of PEMFCs that operate under static conditions. There are also hybrid approaches that combine Kalman filtering with data based neural networks [26]. The main shortcoming in most available stochastic approaches is that they estimate coefficients for a user defined regression curve that models the input-output behavior of the fuel cell. Thus, most available stochastic approaches do not extract the physically meaningful parameters of a model constructed from mechanistic knowledge.

In general, most available studies in fuel cell parameter estimation are focused on finding the parameters of a static polarization curve and if such a model is used by a model-based controller, the found parameters are not updated online when the operating conditions change. Other studies cannot be implemented online, as real-time estimators for a model-based control architecture, due to the computation burden of the algorithm. This is in general the case for bio-inspired optimization. Others do not take into account the uncertainty of the model and the error in the measure of the input-output signals, or they estimate coefficients of an imposed regression curve instead of parameters with physical meaning.

The aim of this study is to fill the research gap for efficient internal state estimation for model-based control of PEMFCs in dynamically changing operating conditions. The main contribution of the study is the development, implementation and testing of a stochastic, control oriented estimator for online continuous tracking of the exchange current density in PEMFCs. The parameter extraction problem is reformulated as a state estimation problem within the theory of stochastic filtering. This approach takes explicitly into account the uncertainty in the model, the changes in the operating conditions and the variability of the parameters. The novel characteristics of the proposed approach are detailed next:

1. The chosen variable to be estimated, the exchange current density, has an important physical meaning from the point of view of control strategies for increasing durability and efficiency of the PEMFC. The exchange current density indicates the capacity of the catalyst to accelerate the

oxygen reduction reaction (ORR). High values of exchange current density indicate a fast and efficient reaction, on the other hand, low values of exchange current density are a sign of a sluggish reaction and higher losses in the activation zone of the voltage-current curve [27]. Also, through the the exchange current density, the electrochemical active surface area of the catalyst (ECSA), a fuel cell state of health indicator, can be estimated.

2. The estimation algorithm employs a mechanistic (or physics-based) model of the fuel cell to continuously estimate the value of the exchange current density, which changes dynamically with the operating conditions. Most past studies on extraction of physical parameters assign a constant value to the exchange current density.

3. The mechanistic expression of the exchange current density is converted into a state transition equation fitted for use in the prediction-correction scheme used in stochastic filtering. This novel step allows the use of stochastic filtering tools for parameter estimation.

4. The stochastic behavior of the model, due to the inherent uncertainty of the parameters and the expected measurement errors of the variables, is taken explicitly into account through the use of a stochastic filtering approach.

5. The filtering algorithm can be implemented online, as the state estimator block of a model-based controller. The estimation of the parameter is done for dynamical operating conditions. The estimation algorithm has been thought explicitly for continuous tracking of the parameter of interest, most other studies focus on static parameter extraction.

6. The estimated exchange current density is used to approximate the value of the ECSA in the cathode catalyst layer.

7. Once the ECSA has been estimated during a training period, its historical values are used to train an ECSA data-driven model with the objective of predicting the trend in ECSA during a prediction period.

The estimation algorithm will be validated with datasets from two different experimental settings. In the case of the first dataset, the particle filter is built from data provided from voltage characterization experiments. A scheme of the estimation approach is shown in Figure 1.

In case of the second database the particle filter is combined with a data-driven identification algorithm with the goal of forecasting the trend of the cell electrochemically active surface area (ECSA). The scheme of the combined approach is depicted in Figure 2. In the estimation/training time interval, the particle filter estimates the exchange current density. This is used to extract the trend of the ECSA and train the data-driven model. Then, in the forecasting time interval, the evolution of ECSA is predicted using future values of the operating conditions.

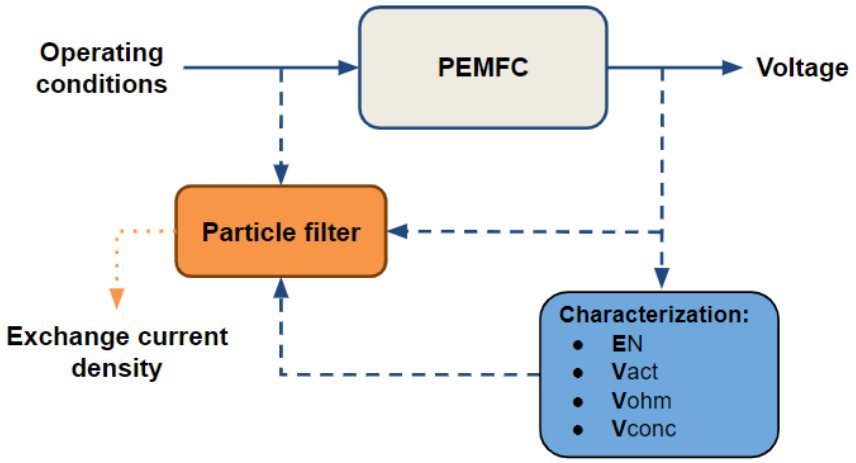

Figure 1: Estimation of the exchange current density through a particle filter.

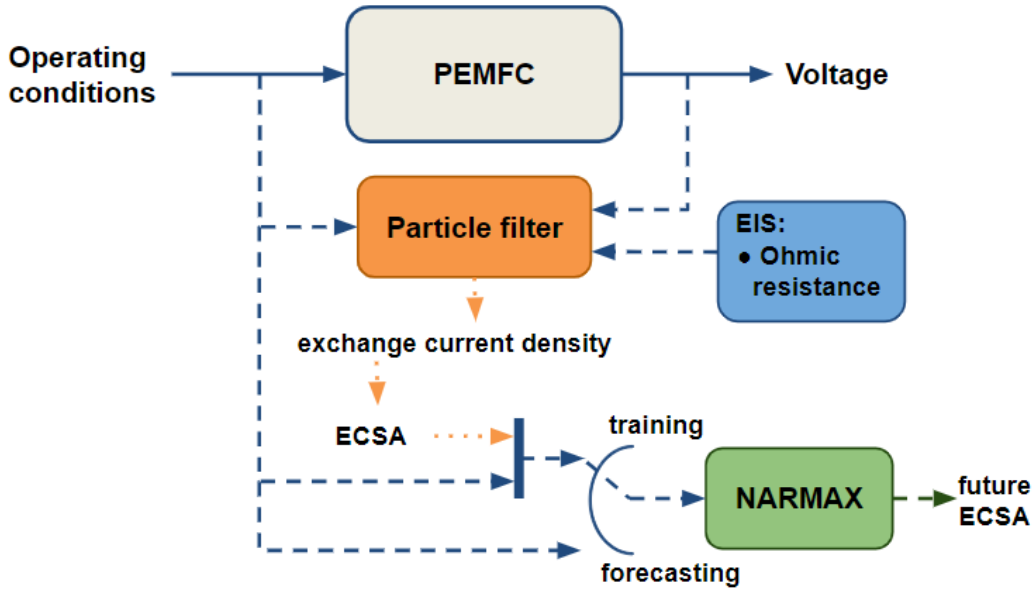

Figure 2: A hybrid structure for state estimation and data-driven forecast

2 PEMFC physics-based model

2.1 Electrochemical dynamics

The stochastic state estimation algorithm is based on the equations derived from fuel cell electrochemical analysis. The cell voltage, v_c, is the result of subtracting a series of voltage losses from a theoretical voltage level [27],

$$v_c = E_N - \frac{RT_{fc}}{\alpha nF}\ln\left(\frac{i_c + i_x}{i_0}\right) - R_{\text{ohm}}(i_c + i_x) + \frac{RT_c}{nF}\ln\left(1 - \frac{i_c + i_x}{i_{\text{lim}}}\right). \quad (1)$$

The cell current density i_c is driven by the load and the operating temperature of the cell T_c is a

variable that can be controlled through an external cooling system.

Eq. (1) is composed of four clearly differentiated expressions: the Nernst voltage E_N, and the voltage losses due to activation v_{act}, ohmic resistance v_{ohm} and reactant concentration v_{con}:

$$v_{\text{act}} = \frac{RT_c}{\alpha nF} \ln\left(\frac{i_c + i_x}{i_0}\right), \tag{2}$$

$$v_{\text{ohm}} = R_{\text{ohm}}(i_c + i_x), \tag{3}$$

$$v_{\text{con}} = \frac{RT_c}{nF} \ln\left(1 - \frac{i_c + i_x}{i_{\text{lim}}}\right), \tag{4}$$

where the cross-over membrane current i_x, the exchange current density i_0, the ohmic cell resistance R_{ohm}, and the limiting current i_{lim} are dynamically changing parameters. The charge transfer coefficient α and the number of attained electrons in the oxygen reduction reaction n are considered static parameters but with a large uncertainty. The ideal gas constant R and the Faraday constant F are constants.

The Nernst voltage depends on the operating cell temperature and the partial pressure of the reactant gases [28],

$$E_N = 1.229 - (8.5 \times 10^{-4})(T_c - T_{\text{ref}}) + (4.3085 \times 10^{-5})T_c(\ln P_{H_2} + 0.5 \ln P_{O_2}), \tag{5}$$

where T_{ref} is the reference temperature (298.15 K), P_{O_2} is the oxygen partial pressure in the cathode and P_{H_2} is the hydrogen partial pressure in the anode.

The exchange current density depends on operating conditions such cell temperature and oxygen partial pressure:

$$i_0 = i_{0\text{ref}} A_c L_{Pt} \left(\frac{P_{O_2}}{P_{\text{ref}}}\right)^{0.5} e^{\left[\frac{-\Delta G}{RT_c}\left(1 - \frac{T_c}{T_{\text{ref}}}\right)\right]}. \tag{6}$$

L_{Pt} is the platinum loading in the catalyst layer in units of mg_{Pt}/cm^2, A_c is the active catalyst area (ECSA) in cm^2/mg_{Pt}, $i_{0\text{ref}}$ is the reference exchange current density, a material-specific constant parameter, and ΔG is the Gibbs activation energy [29]. It has been widely proved that the exchange current density in the anode in a hydrogen fuel cell is three to four orders of magnitude larger than the exchange current density in the cathode, so the losses associated to activation energy in the anode are negligible [27]. Only the cathode activation losses are taken into account in this paper.

3 Stochastic State Estimation

3.1 Exchange current density dynamics as a hidden Markov model

A stochastic system model includes a state transition function $f(\cdot)$ and a measurement (or observation) function $g(\cdot)$. The state transition equation propagates states through time, mapping current states x_t, inputs u_t and process model noise v_t to future states x_{t+1}. The measurement function relates the system measured outputs y_t to the system internal states, the external inputs and observation noise w_t. Modelling the process noise and the observation noise is the fundamental difference between the stochastic and the deterministic approach in system analysis.

$$\begin{aligned} x_{t+1} &= f(x_t, u_t, v_t) \\ y_t &= g(x_t, u_t, w_t). \end{aligned} \tag{7}$$

The process noise term seeks to capture the errors in the model derived from the uncertainty in the parameters and the unmodeled internal dynamics, while the output noise term represents the noise in the measurement.

The particle filter state estimation algorithm is a generalization of the sequential importance resampling algorithm [30]. Particle filtering is a stochastic, non-optimal, Monte Carlo method [31] that seeks to overcome the limitations of the well known family of Kalman filters. Such limitations include the requirement of linearity of the system and the assumption that all variables have a Gaussian probability distribution in the case of the Kalman filter; the requirement of system linearization in the extended Kalman filter; or the requirement of nonlinear Gaussian fitting at each step in the unscented Kalman filter [32].

However, for all its advantages, particle filters have some drawbacks that have to addressed in the implementation algorithm. An important drawback is the the particle degeneracy problem. This occur when one particle has a weight close to one while all the other particles have weights close to zero. Several improvements in the basic particle filter algorithm can be implemented to cope with this and other drawbacks [33].

In the context of stochastic state estimation, a system defined following the structure of Eq. (7) can be framed as a hidden Markov model (HMM). In the case of the present PEMFC model the resulting input-output hidden Markov model, is built from Eqs. (1) and (6), where the exchange current density is the hidden state that depends exclusively on the the present input values and the immediately previous state.

3.2 Particle filter for estimation of the exchange current density

This paper propose a particle filter for the estimation of the exchange current density of PEMFCs operating under dynamic conditions. Eqs. (1) and (5) form the observation model, and Eq. (6), which relates the inputs to the hidden state, is the precursor of the state transition function. Since Eq. (6) is a static equation it must be transformed into an appropriate state transition form in order to apply the HMM framework.

Deriving (6) with respect to time results in the following expression:

$$\frac{di_0}{dt} = i_{0_{\text{ref}}} A_c L_{Pt} e^{\left[\frac{-\Delta G}{RT_c}\left(1-\frac{T_c}{T_{\text{ref}}}\right)\right]}\left[\gamma\left(\frac{P_{O_2}}{P_{O_{2_{\text{ref}}}}}\right)^{\gamma-1}\frac{dP_{O_2}}{dt} + \left(\frac{P_{O_2}}{P_{O_{2_{\text{ref}}}}}\right)^{\gamma}\left(\frac{1}{T_c^2}\right)\frac{dT_c}{dt}\right]. \tag{8}$$

The state transition equation is obtained by discretizing the time derivatives in Eq. 8 through backward difference approximation ($\frac{dx}{dt} \approx \frac{x_t - x_{t-1}}{\Delta t}$):

$$i_{0_t} = i_{0_{t-1}} + i_{0_{\text{ref}}} A_c L_{Pt} e^{\left[\frac{-\Delta G}{RT_c}\left(1-\frac{T_c}{T_{\text{ref}}}\right)\right]}\left[\gamma\left(\frac{P_{O_2}}{P_{O_{2_{\text{ref}}}}}\right)^{\gamma-1}\Delta P_{O_2} + \left(\frac{P_{O_2}}{P_{O_{2_{\text{ref}}}}}\right)^{\gamma}\left(\frac{1}{T^2}\right)\Delta T_c\right], \tag{9}$$

where $\Delta T_c = T_{c_t} - T_{c_{t-1}}$ and $\Delta P_{O_2} = P_{O_{2_t}} - P_{O_{2_{t-1}}}$.

Thus, the state transition function and the measurement function used in the particle filter state estimation algorithm are expressed in Eqs. (9) and (1) respectively. The proposed algorithm for estimating the exchange current density as a hidden state of the PEMFC system is shown in Algorithm 1.

Algorithm 1 Particle filter for estimation of exchange current density

Define the estimation period and the number of particles
$N \leftarrow$ number of particles
$T \leftarrow$ total estimation time
$t \leftarrow 0$ initialize time
Initialize the particle filter distribution
for $i = 1....N$ **do**
  $T^i \sim \mathcal{N}(T_c, \sigma_{T_c})$ generate N samples of T_c from defined distribution
  $P^i_{O_2} \sim \mathcal{N}(P_{O_2}, \sigma_{P_{O_2}})$ generate N samples of P_{O_2} from defined distribution
  $i^i_0 \sim p(i_0|T^i)$ generate N initial particles of i_0 through Eq. 6
  $w^i_t \sim \mathscr{U}$(0,N) generate normalized weight for each particle from defined distribution
end for
Hidden state estimation loop
for $t = 1 : T$ **do**
  for $i = 1 : N$ **do**
    $i^i_{0_t} = f(i_{0_{t-1}}, i, T_c)$ update particles through state transition function Eq. 9
    $v^i_{c_t} = h(i^i_{0_t}, i_{c_t}, T_{c_t})$ calculate output through measurement function Eq. 1
    $w^i_t \propto w^i_{t-1} * p(v_{c_t}|i_{0_t})$ estimate weights through likelihood function
  end for
  $\hat{i}_{0_t} = \sum_i i^i_{0_t} w^i_t$ define estimated value of i_0
  $i^i_{0_t} \sim i^i_{0_t}, w^i_t$ re-sample particles according to weights
end for

First, at $t = 0s$, the number of particles N and the total estimation time T are defined. Then N samples are drawn from Gaussian distributions of cell temperature and oxygen partial pressure. Next, N

exchange current density particles are created from the temperature and oxygen partial pressures samples through static equation Eq. (6). Then, at $t = 1s$, every i_0 particle is updated through the state transition Eq. (9) and for each of these particles a corresponding output voltage is computed. Next, weights are assigned to every i_0 particle by the likelihood function $p(v_c|i_0^i)$ that compares, through Eq. (1), the output produced by every exchange current density particle with the actual observed output at that time instant. The set of particles and its corresponding weights form the estimated posterior distribution of the exchange current density in the current time step. The estimated value of i_0 at the current time step is calculated as the weighted mean of the estimated posterior distribution. This distribution is resampled based on particle weights. The set of resampled particles serves as input for the next time step. The loop is repeated until $t = T$.

4 Data-driven modelling

There is an increasing interest in complementing physics-based models (also called first principles models) with model structures built exclusively from data. These hybrid architectures aim to take advantage of the respective strength in the physics-based and data-driven approach, in order to represent complex behavior, system non-linearities, non stationary dynamics or time varying parameters. Hybrid approaches have been proposed to estimate the remaining useful life of lithium ion batteries, where the algorithm is composed of a Kalman filter and a multi layer neural network [34], the Kalman filter estimates the hidden internal states while the neural network serves as the observation expression, forecasting future values of the output variable. Also, a parallel structure of neural network and Kalman filter has been proposed to estimate and forecast system hidden states. [35]

This paper presents a hybrid architecture where the values of the ECSA, computed from the estimation of the exchange current density during a training period, are used to obtain a nonlinear auto-regressive moving average with exogenous inputs model (NARMAX).

4.1 The NARMAX structure

The NARMAX models were introduced as an extension of the classical linear auto-regressive models [36, 37]. The general NARMAX structure, Eq. (10), is composed of a vector of regressors of the outputs $y(t)$, inputs $u(t)$ and estimation error $e(t)$, a vector of constant coefficients Θ, and a non linear function $F(\cdot)$. The parameters n_a, n_b and n_c define the order of delay of the output, input and error regressors respectively. The non linear function is some user defined basis function such as wavelets, sigmoids or even a full neural network. The elements of the regressor vector can be polynomials of different order of the regressor element, including cross-products and rationals or, in general, nonlinear functions such as trigonometric or exponential functions. It is worth to note that, in all those cases, the model is linear in

the coefficients.

$$\mathbf{y}(t) = F(\Theta * [\mathbf{y}(t-1), ..., \mathbf{y}(t-n_a), \mathbf{u}(t), ..., \mathbf{u}(t-n_b), \mathbf{e}(t), ..., \mathbf{e}(t-n_c)]). \tag{10}$$

NARMAX model construction is done by choosing candidate elements for the regressor vector and then computing the coefficient through an appropriate least squares optimization algorithm. The candidate regressor elements which, as stated earlier, can be single element regressors, polynomials or regressor functions, can be selected based on the knowledge of the dynamics of the system. This is a fundamental advantage of NARMAX models since this approach produces transparent, easy to interpret models, where mechanistic knowledge about the interaction of the system variables can be included.

4.2 NARMAX model for tracking ECSA profile

When the exchange current density is estimated and tracked online, it can be used with Eq. (6) and the knowledge of the specific conditions of operation of the fuel cell, to extract the value of the ECSA.

ECSA models have established that its decay rate is highly dependant on the operating conditions of the fuel cell, such as temperature, the relative humidity of the reactant gases or the profile of load current [4, 5]. The analytical expressions of ECSA as a function of time and operating conditions are hard to fit and require extensive experiments. This study proposes to compute the ECSA, through the estimation of the exchange current density, during a training period, then this time series of ECSA values is used to train a data-driven model with the objective of forecasting ECSA evolution in the future. This approach allows to overcome the complexity of computing the ECSA through complex models that require the tuning of many other parameters.

The proposed regressor vector of the NARMAX model is presented in Eq. (11). The inputs of the model are the operating time, the fuel cell temperature and relative humidity of the inlet air, also, in order to increase robustness of the prediction, past values of ECSA (auto-regressor element) are taking into account by the model. All the elements in the regressor vector are linear with delay order of two and wavelet functions are used as the nonlinear mapping. The NARMAX coefficients are computed through the orthogonal least squares algorithm.

$$\mathbf{x}(t) = \Big[y(t-1), y(t-2), u_1(t), u_1(t-1), u_2(t), u_2(t-1), u_3(t), u_3(t-1)\Big], \tag{11}$$

where,

$$y(t) = ECSA(t) \quad \text{and} \quad \mathbf{u}(t) = \begin{bmatrix} time(t) \\ T_c(t) \\ RH_{air,\text{in}}(t) \end{bmatrix}.$$

5 Experimental conditions and datasets

The state estimation approach is tested in two scenarios. In the first case, the data is obtained from a single cell operated in semi-dynamic conditions. Characterization experiments are done in the fuel cell in order to obtain the values of voltages corresponding to each component of Eq. (1). This dataset was originally produced as part of fuel cell characterization studies carried on within the PUMA-MIND European Project of the FP-7 Fuel Cell and Hydrogen Joint Undertaking [38].

The fuel cell voltage characterization was done through the procedure of current interrupt and current sweep [38]. A Horizon H-100 open cathode, 20 cell, 22.5 cm2 active area fuel cell stack was tested on a controlled environmental chamber. A constant flow of pure, dry hydrogen was supplied to the stack. The environmental chamber was set to an ambient temperature of 25^{o}C and a relative humidity of 90%. Cell temperature and current were changed dynamically. Cell temperature was controlled through speed control of a cooling fan and cell current was controlled through an adjustable electrical load.

The experimental values of Nernst voltage E_N, activation overpotential v_{act}, ohmic overpotential v_{ohm} and concentration overpotential v_{con} are used to estimate the exchange current density through the particle filter algorithm described in section 3.3. The estimation scheme is shown in Figure 1. The profiles of voltage, current, temperature and experimentally characterized voltage losses are shown in Figure 3.

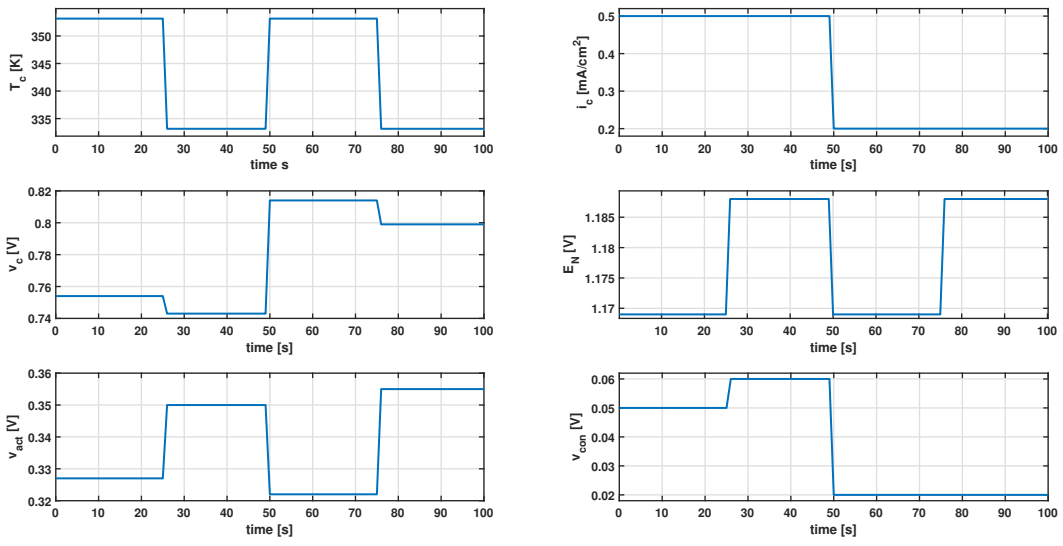

Figure 3: Temperature, current density, cell voltage and voltage losses in the first dataset

In the second case, the behavior of a cell within a five cell stack is analyzed. The value of ohmic resistance R_{ohm} is obtained regularly during the test through experimental characterization. This dataset was produced by the FCLAB Research Center in Belfort, France for the 2014 IEEE Prognosis and Health Management Data Challenge.

The five cell stack was subjected to a degradation test for a period of approximately 1000 hours. For

the purpose of validating the approach proposed by this study, a total of 786 hours of data from the aforementioned dataset is used. The profiles of cell voltage, current density, temperature and inlet air relative humidity are shown in Figure 4. An exponential moving average filter with a window of 1000 samples is applied to the original cell voltage. This filtered signal will be used as the experimental cell voltage v_c, for the rest of the analysis.

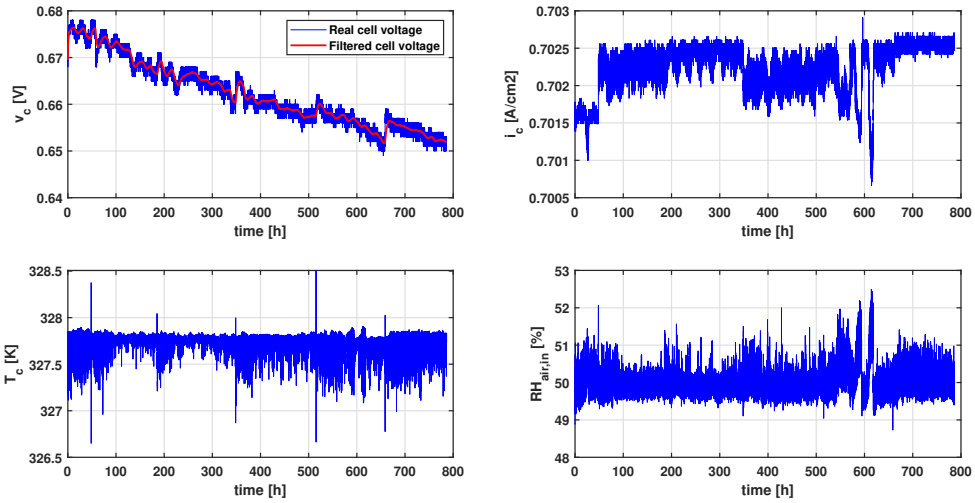

Figure 4: Profiles of cell voltage, current density, cell temperature and relative humidity in the second dataset

The operating conditions are kept constant and polarization and electrochemical impedance spectroscopy (EIS) tests were performed at regular time intervals (approximately every 168 hours) to determine the state of health of the stack. The details of the test setting, characterization procedure and goal of the challenge are described also in [24]. Figure 5 shows the results of polarization test at the start (BOL) and at the end of the degradation test (EOL).

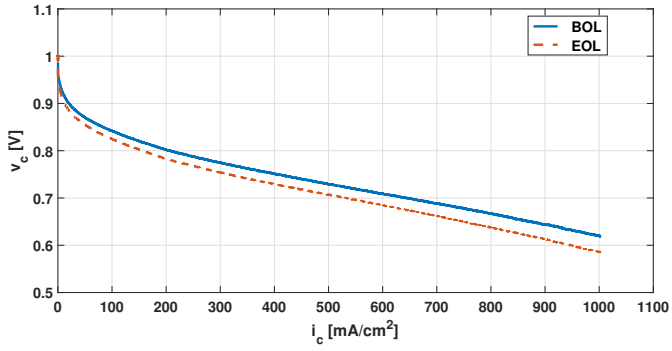

Figure 5: Polarization curves at BOL and EOL

Information about impedance associated with ohmic resistance and catalytic activity can be extracted from the Nyquist plot of the EIS. The evolution in ohmic resistance is presented in Figure 6.

Once the exchange current density is estimated, it is used to approximate the trend of decay in ECSA

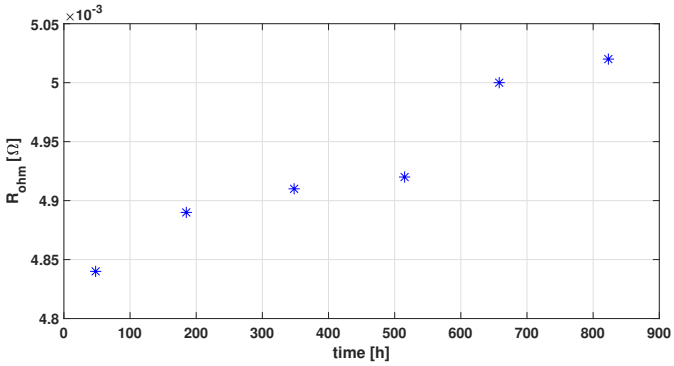

Figure 6: Change of the ohmic resistance along the degradation test.

and build a NARMAX model to forecast ECSA future evolution. The estimation and tracking scheme is shown in Figure 2.

6 Results and discussion

6.1 Case 1: Estimation of exchange current density from a voltage losses characterisation dataset

The particle filter in Algorithm 1, built from the physics-based model, Eq. (1) and Eq. (9), approximates the posterior probability distribution of the exchange current density. The validation of the estimated value of the exchange current density is done by using this value to reconstruct the measured fuel cell voltage and the relative error between real cell voltage and the voltage reconstructed from the estimated exchange current density is computed. The estimated and experimental values of exchange current density and cell voltage as well as the voltage estimation error is shown in Figure 7.

6.2 Case 2: Estimation of exchange current density from a degradation characterisation dataset

In the case of the second dataset, in order to construct the observation equation of the particle filter, an approximation of the voltage concentration losses, the ohmic resistance and the Nernst voltage is performed. It can be seen, from the polarization curves, that there is not significant change in the value of the limiting current (1000 mA/cm^2). Then, it can be assumed that the concentration overpotential component in Eq. (4) has not increased in the operating region of interest and thus this term does not contribute to the voltage decay.

The evolution in ohmic resistance, as shown in Figure 6, can be approximated by a linear curve. Then, by interpolation along this curve, values of R_{ohm} can be sampled at any given time. These values are used to compute the voltage losses associated with ohmic resistance at any time instant.

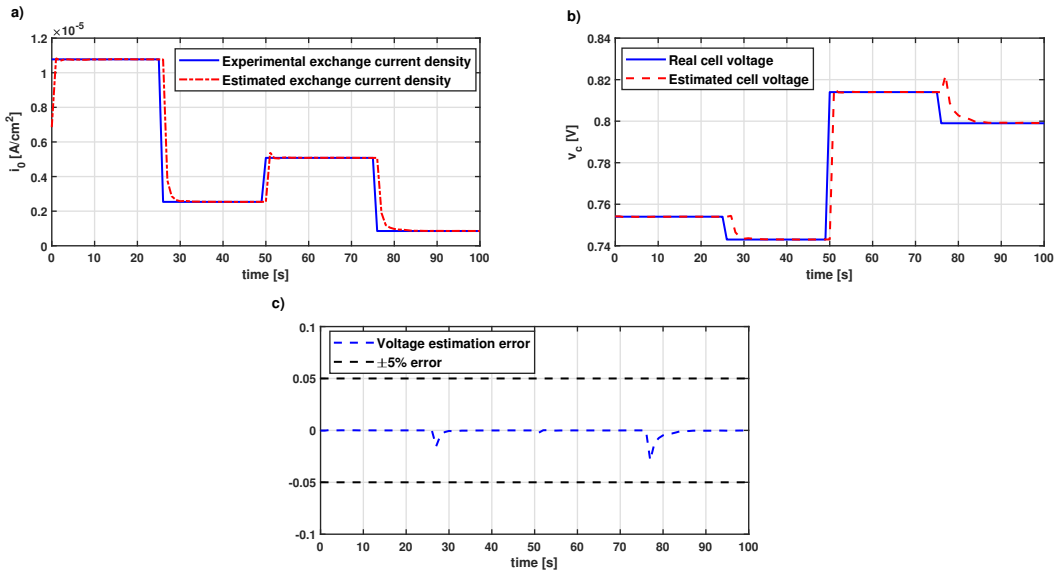

Figure 7: Comparison of estimated and experimental values of exchange current density (a) and cell voltage (b). Resultant voltage relative estimation error (c).

In order to complete the components of the observation equation of the particle filter, Eq. (1), an approximation of the Nernst voltage is done from Eq. (5). The hydrogen partial pressure P_{H_2} is approximated by the value of output anode pressure provided in the experimental dataset. The oxygen partial partial pressure P_{O_2} is derived from the following mass balance analysis:

$$\frac{P_{O_2}}{P_{\text{out}}} = \frac{\dot{n}_{O_2}}{\dot{n}_{O_2} + \dot{n}_{N_2} + \dot{n}_v}. \tag{12}$$

Being $\dot{n}_{O_2}$, $\dot{n}_{N_2}$ and $\dot{n}_v$ the total molar flows of oxygen, nitrogen and vapor in the cathode respectively. P_{out} is the total pressure of the air exiting the cathode, this value is provided in the dataset. The total flows of oxygen, nitrogen and water vapor are defined in Eqs. (13), (15) and (15) respectively:

$$\dot{n}_{O_2} = \dot{n}_{O_2,\text{in}} - \dot{n}_{O_2,\text{ORR}}, \tag{13}$$

$$\dot{n}_v = \dot{n}_{v,\text{in}} + \dot{n}_{v,\text{ORR}}, \tag{14}$$

$$\dot{n}_{N_2} = \dot{n}_{N_2,\text{in}}, \tag{15}$$

where $\dot{n}_{O_2,\text{in}}$, $\dot{n}_{N_2,\text{in}}$ and $\dot{n}_{v,\text{in}}$ are the inlet molar flows of oxygen, nitrogen and water vapor going into the cathode respectively; $\dot{n}_{O_2,\text{ORR}}$ and $\dot{n}_{v,\text{ORR}}$ are the oxygen consumed and the water vapor produced by the ORR respectively. The inlet molar flow of vapor can be computed from the values of inlet

air temperature and inlet air relative humidity provided in the dataset. First, the vapor saturation pressure and the vapor pressure of the air entering the cathode are computed through Eqs. (16) and (17) respectively,

$$P_{sat,air,\text{in}} = p_0 e^{\left(\frac{-E_v}{RT_{air,\text{in}}}\right)}, \tag{16}$$

$$P_{v,\text{in}} = RH_{air,\text{in}} P_{sat,air,\text{in}}, \tag{17}$$

where $P_{sat,air,\text{in}}$ is the vapor saturation pressure, $P_{v,\text{in}}$ is the vapor pressure, $T_{air,\text{in}}$ is the temperature and $RH_{air,\text{in}}$ is the relative humidity of the inlet air. Then the partial pressure of the dry part of inlet air $P_{dry,\text{in}}$ and molar mass mass of the dry part of inlet air are computed through Eqs. (18) and (19):

$$P_{dry,\text{in}} = P_{air,\text{in}} - P_{v,\text{in}}, \tag{18}$$

$$M_{dry} = 0.21 M_{O_2} + 0.79 M_{N_2} \tag{19}$$

The humidity ratio, computed through Eq. (20), is used to calculate the molar flow of vapor entering the cathode $\dot{n}_{v,\text{in}}$, Eqs. (21) to (23):

$$w_{ca} = \frac{M_v}{M_{dry}} \frac{P_{v,\text{in}}}{P_{dry,\text{in}}}, \tag{20}$$

$$\dot{m}_{dry,\text{in}} = \frac{1}{1 + w_{ca}} \dot{m}_{air,\text{in}}, \tag{21}$$

$$\dot{m}_{v,\text{in}} = \dot{m}_{air,\text{in}} - \dot{m}_{dry,\text{in}}, \tag{22}$$

$$\dot{n}_{v,\text{in}} = \frac{\dot{m}_{v,\text{in}}}{M_v}. \tag{23}$$

The vapor produced in the ORR is computed through Eq. (24),

$$\dot{n}_{v,\text{ORR}} = \frac{nI_c}{2F}. \tag{24}$$

The total oxygen molar flow is computed in a similar manner, Eqs. (25) to (27):

$$\dot{m}_{O_2,\text{in}} = x_{O_2,\text{in}} \dot{m}_{dry,\text{in}}. \tag{25}$$

Where $x_{O_2,\text{in}}$ is the mass fraction of oxygen in dry air. Then the molar flows of inlet oxygen and oxygen consumed in the ORR are:

$$\dot{n}_{O_2,\text{in}} = \frac{\dot{m}_{N2,\text{in}}}{M_{O_2}}, \tag{26}$$

$$\dot{n}_{O_2,\text{ORR}} = \frac{nI_c}{4F}. \tag{27}$$

The values and units of constants used in the equations (12) to (27) are shown in Table 2. The approximation proposed for P_{O_2} may have, in the range of operation of the fuel cell under study, an estimation error of around 10% [17]. An analysis of the expression for the Nernst voltage, Eq. (5), shows that even errors in the order 20% in the estimation of the oxygen partial pressure produce errors of around 1% in the computed value of the Nernst voltage. In the case of the exchange current density, a 20% error in the estimation of oxygen partial pressure results in an error of around 10% in i_0. Then, it is concluded that the approximation of P_{O_2} is within the range of values that can be corrected by the particle filter.

Once the Nernst voltage has been approximated, the exchange current density can be estimated by the particle filter algorithm, Algorithm 1. Figure 8 shows the the estimated profile of the exchange current density.

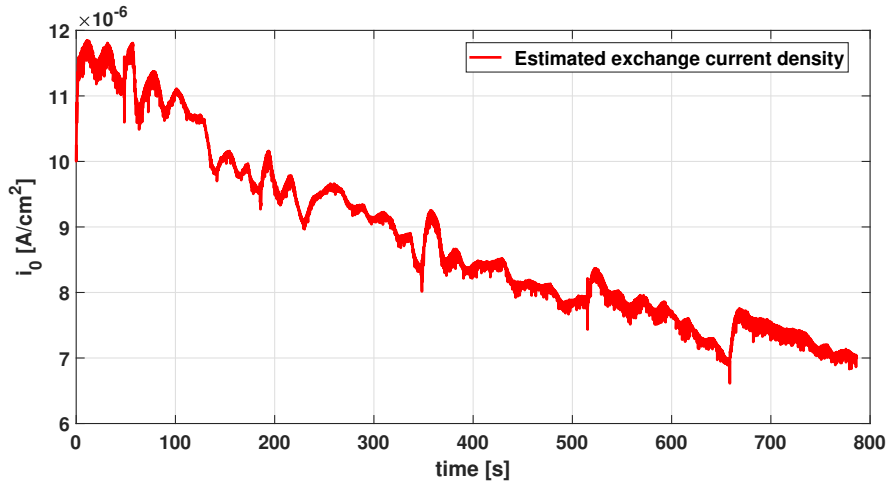

Figure 8: Estimated profile of the exchange current density.

The objective of the particle filter is to approximate the posterior probability distribution of the hidden state of a stochastic system making use of prior model knowledge and posterior observations. Figure 9a presents the estimated distribution of the exchange current density at the beginning of the estimation time. Then, once the filter is implemented, the estimated distribution at the end of the estimation time is shown in Figure 9b.

The time distribution of the particles corresponding to the shown the distributions is presented in

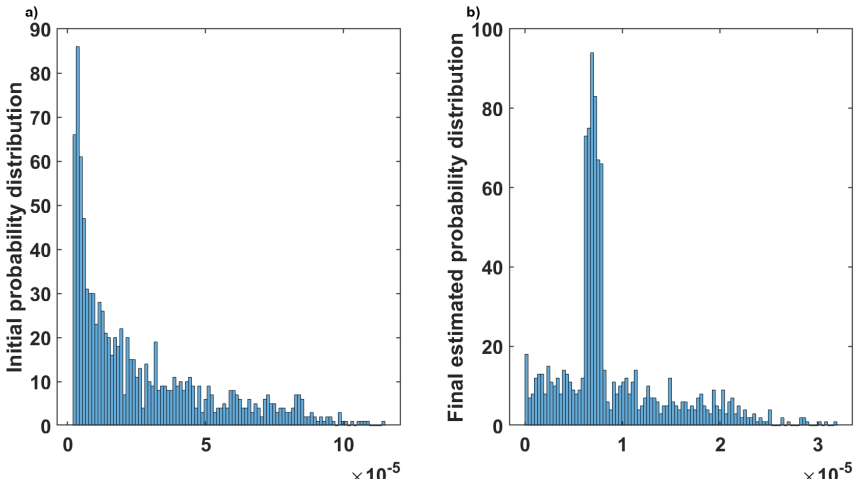

Figure 9: Initial and final distribution of the exchange current density

Figure 10. It can be seen that the wide prior distribution of particles is narrowed by the filter through the estimation period resulting in a better confidence of the estimation.

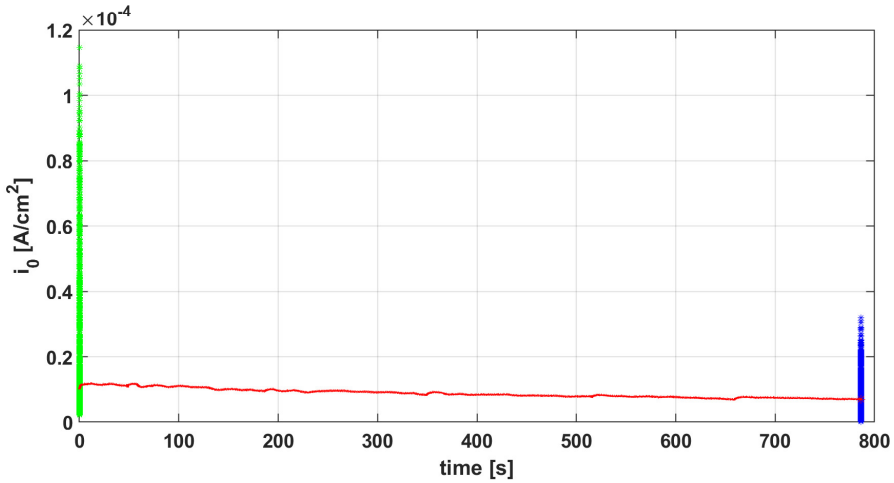

Figure 10: Particles at the beginning and at the end of the estimation period

The estimation of i_0 is validated by the reconstruction of the cell voltage using the measurement equation. Figure 11 shows the comparison between the real cell voltage and the reconstruction obtained through the estimated exchange current density. It can be seen that the particle filter is able to follow the value of the real voltage and overcome the noise in the measurement of the operating variables and also the uncertainties in the parameters of the state transition equation.

The error in the voltage reconstruction from the estimated exchange current density, is in the order of 10^{-4} volts, Figure 12. This result can be compared with previous works. As stated in section 1, nonlinear parameter observers (NPO) [39] and high order sliding mode observers (HOSM) [17] have been proposed for online estimation and continuous tracking of dynamically changing parameters (or internal states) in PEMFCs. It is worth to mention that these studies asses the performance of its proposal by comparing

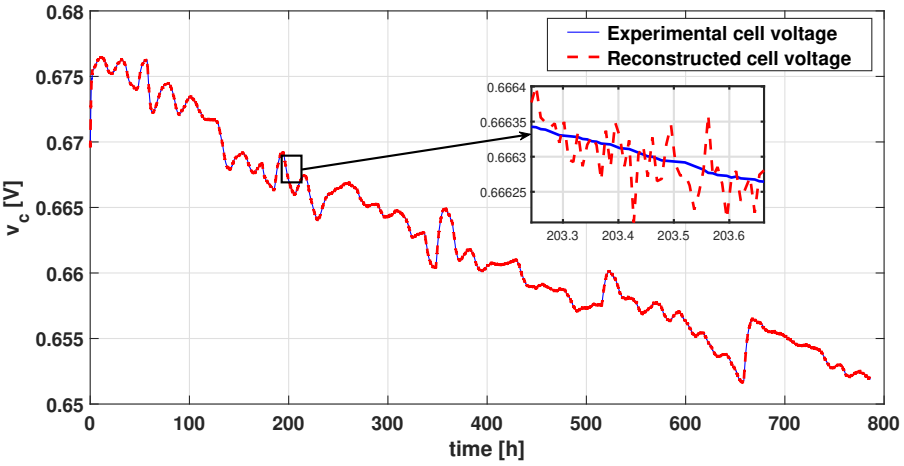

Figure 11: Experimental cell voltage and reconstructed voltage from the estimated exchange current density.

the values of parameters obtained through simulation from a complex fuel cell models, with the value estimated from the simpler model used in the estimation algorithm. This is due to the fact that the real value of the parameter of interest is hard or even impossible to measure in a real fuel cell. The approach of this study, on the other hand, is to use the estimated parameter to reconstruct the measured observation (the cell voltage) and compare the reconstruction with the observed real value. Table 1 presents the reported mean absolute error (MAE) of the estimation in previous works (the comparison of simulated parameter values with estimated parameter values) and the MEA of the voltage reconstruction in the present study.

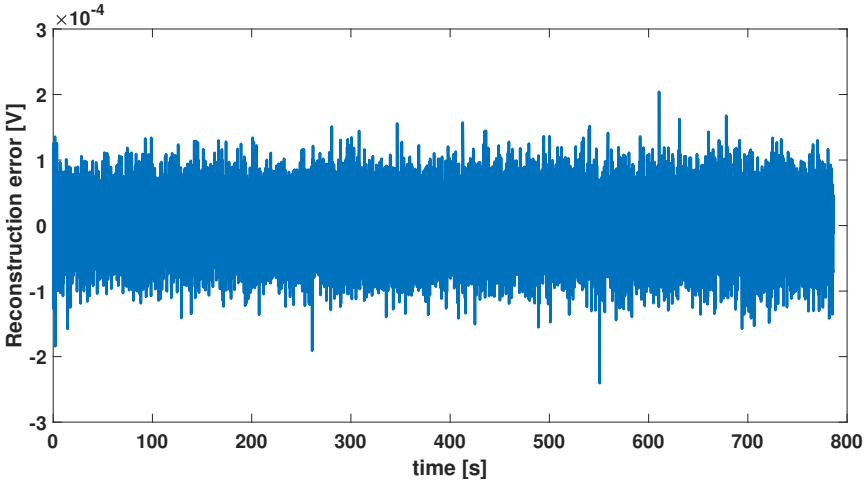

Figure 12: Voltage reconstruction error.

The exchange current density equation, allows to extract the parameter that is presumed to be the main cause of the degradation in cell performance within the experimental setting under study. The trend of ECSA, A_c in Eq. (6), can be estimated through Eq. (28), taking into account that the goal is the approximation of the irreversible degradation trend and that the operating conditions are constant

	NPO	HOSM	PF
MAE	0.0178	0.0154	0.0043

Table 1: Mean absolute error of estimation algorithms

during the entire period of the experiment.

$$\frac{ECSA_t}{ECSA_{t=0}} = \frac{i_{0_t}}{i_{0_{t=0}}} \tag{28}$$

ECSA decay is a process caused by several factors. It has been modelled by complex expressions that require the extraction or assumption of many parameters [3–5]. The approach proposed by this study is to approximate ECSA through the exchange current density. Even though the operating conditions, fuel cell characteristics and experimental settings of the dataset used in this paper are different from the ones in the referenced studies, which impedes an exact comparison of ECSA values, the decreasing exponential shape in the computed ECSA profile of this paper coincides qualitatively with those studies. A further analysis serves to illustrate how an online estimation of exchange current density and ECSA can be used to take predictive control actions for increasing fuel cell durability.

A subset of data (366 hours, the gray region in Figure 13) is used to estimate the coefficients of the NARMAX structure described in section 4. The NARMAX model is used to forecast the evolution of ECSA after the training period, knowing the future operating conditions. It is worth to point out that, unlike previous studies on degradation forecasting mentioned in section 1, the predictive model proposed in this study incorporates information of the input operating conditions to forecast the ECSA trend. Figure 14 shows the modelling relative error ϵ_{ECSA} given by the NARMAX model. The model is able to successfully approximate and predict, for a long period of time, the trend of ECSA.

Finally a simulated scenario is produced to approximate the response of the ECSA profile to different operating conditions. Figure 15 shows the predicted evolution of ECSA for temperature values of $\pm 25K$. The predicted profiles agree qualitatively with results presented in the studies referred in section 1.

Symbol	Description	Value	Units
p_0	Fitting pressure coefficient	30.05	GPa
E_v	Vapor energy	36.98	kJ mol^{-1}
R	Gas constant	8.314	J molK^{-1}
M_{O_2}	Oxygen molar mass	32x10^{-3}	kg mol^{-1}
M_{N_2}	Nitrogen molar mass	28x10^{-3}	kg mol^{-1}
M_v	Water vapor molar mass	18x10^{-3}	kg mol^{-1}

Table 2: Values and units of the constants

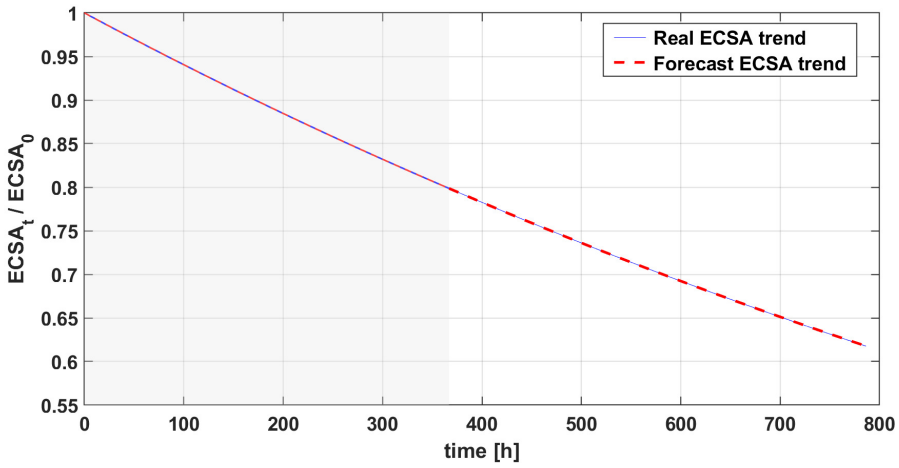

Figure 13: ECSA trend computed from the estimated exchange current density and identified by the NARMAX approach.

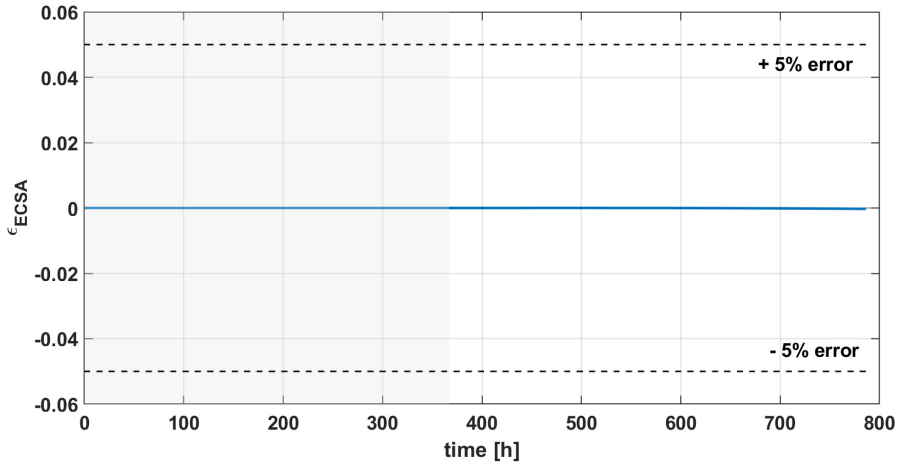

Figure 14: Relative modelling error of the NARMAX model.

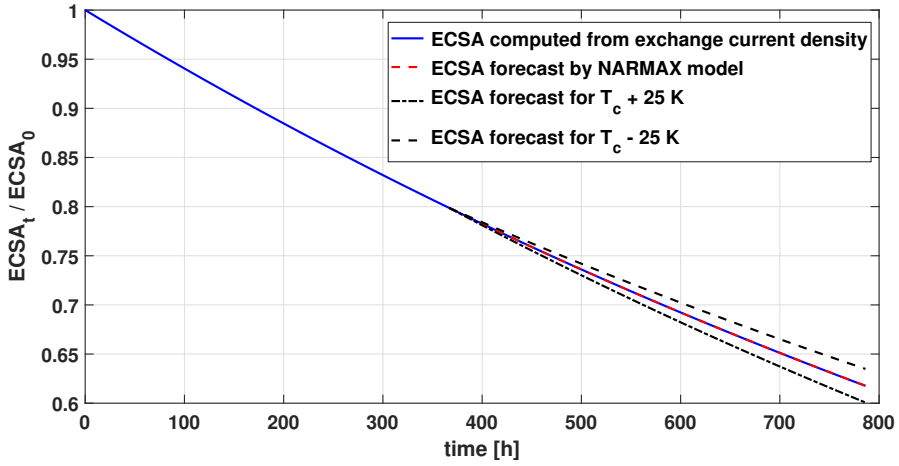

Figure 15: Trend of ECSA and simulated evolution of ECSA for different cell temperatures.

7 Conclusions

This study developed, implemented and tested a novel approach for online estimation of the exchange current density in PEMFCs operating under dynamical conditions. The fuel cell was framed as an input-output hidden Markov model where the parameter of interest, the exchange current density, is the hidden state. This procedure allows for the use of stochastic filtering for state estimation. The estimation algorithm, based on a particle filter, was able to cope with non-linearities and non-Gaussian behavior of the model.

The proposed state estimator has been successfully validated through two datasets from different experimental settings. In the first dataset the exchange current density was estimated from the voltage signal and information from voltage losses characterization experiments, with dynamical operating conditions of current and temperature. In the second dataset, from a degradation analysis experiment, the state estimation algorithm was combined with a data-driven, auto-regressive model to forecast the dynamical evolution of the electrochemical active surface area in the cathode's catalyst. Knowing the instantaneous values of the exchange current density, the ECSA was computed and tracked for a period of time. The values of ECSA during the tracking period were used to train an auto-regressive model. This auto-regressive model was then used to forecast the evolution of the ECSA. This shows that efficient continuous tracking of the exchange current density can lead to a better forecasting of cell durability. In a further step, different profiles of fuel cell temperature were simulated to analyze the behavior in ECSA evolution.

Future work will focus on testing the algorithm with more datasets, under a higher range of dynamical changes in the operating conditions and finally on implementing the proposed approach as state estimator within a state based control architecture.

Acknowledgements

This work is supported by the Project MDM-2016-0656 and the program "ESF Investing in your future" [grand number BES-2017-082441] funded by MCIN/AEI /10.13039/501100011033, by the European Union through the INN-BALANCE project of the Fuel Cells and Hydrogen 2 Joint Undertaking [grant number 735969], and by the contract GEPEVE: Gestión predictiva de energía para eficiencia energética en vehículos eléctricos con control de crucero adaptativo of the Movilidad 2030 project of the 2020 Misiones CDTI program.

Conflict of interests

The authors declare that there is no conflict of interest and no financial competing interests.

Data availability statement

The data that support the findings of this study are available on request from the corresponding author.

References

[1] U.S. Department of Energy, Fuel Cell Technologies Office, "Multi-year research, development, and demonstration plan," 2014. www.energy.gov/eere/fuelcells/downloads/hydrogen-and-fuel-cell-technologies-office-multi-year-research-development.

[2] R. Darling and J. Meyers, "Kinetic model of platinum dissolution in PEMFCs," *Journal of the Electrochemical Society*, vol. 150, no. 11, pp. A1523–A1527, 2003.

[3] A. Pandy, Z. Yang, M. Gummall, V. Atrazhev, N. Y. Kuzminyh, V. Sultanov, and S. Burlatskyb, "A carbon corrosion model to evaluate the effect of steady state and transient operation of a polymer electrolyte membrane fuel cell," *Journal of the Electrochemical Society*, vol. 160, no. 9, pp. F972–F979, 2013.

[4] P. Schneider, C. Sadeler, A. Scherzer, N. Zamel, and D. Gerteisen, "Fast and reliable state-of-health model of a PEM cathode catalyst layer," *Journal of The Electrochemical Society*, vol. 166, no. 4, pp. F322–F333, 2019.

[5] A. Kneer and N. Wagner, "A semi-empirical catalyst degradation model based on voltage cycling under automotive operating conditions in PEM fuel cells," *Journal of The Electrochemical Society*, vol. 166, no. 2, pp. F120–F127, 2019.

[6] O. Hachana, "Accurate PEM fuel cells parameters estimation using hybrid artificial bee colony differential evolution shuffled complex optimizer," *International Journal of Energy Research*, vol. 45, no. 5, pp. 6383–6405, 2022.

[7] J. Shen, C. Du, F. Yan, B. Chen, and Z. Tu, "Two parameters identification for polarization curve fitting of PEMFC based on genetic algorithm," *International Journal of Energy Research*, vol. 46, no. 7, pp. 9621– 9633, 2022.

[8] S. I. Selem1, H. M. Hasanien, and A. A. El-Fergany, "Parameters extraction of PEMFC's model using manta rays foraging optimizer," *International Journal of Energy Research*, vol. 44, no. 6, pp. 4629–4640, 2020.

[9] M. A. M. Shaheen, H. M. Hasanien, M. S. E. Moursi, and A. A. El-Fergany, "Precise modeling of PEM fuel cell using improved chaotic Mayfly optimization algorithm," *International Journal of Energy Research*, vol. 45, no. 13, pp. 18754–18769, 2021.

[10] D. Kler, K. P. S. Rana, and V. Kumar, "Parameter extraction of fuel cells using hybrid interior search algorithm," *International Journal of Energy Research*, vol. 43, no. 7, pp. 2854–2880, 2019.

[11] M. Abdel-Basset, R. Mohamed, and V. Chang, "An efficient parameter estimation algorithm for proton exchange membrane fuel cells," *Energies*, vol. 14, no. 21, 2021.

[12] Y. Chen, D. Pi, B. Wang, J. Chen, and Y. Xu, "Bi-subgroup optimization algorithm for parameter estimation of a pemfc model," *Expert Systems with Applications*, vol. 196, p. 116646, 2022.

[13] Y. Zhu and N. Yousefi, "Optimal parameter identification of PEMFC stacks using adaptive sparrow search algorithm," *International Journal of Hydrogen Energy*, vol. 46, no. 14, pp. 9541–9552, 2021.

[14] M. T. Özdemir, "Optimal parameter estimation of polymer electrolyte membrane fuel cells model with chaos embedded particle swarm optimization," *International Journal of Hydrogen Energy*, vol. 46, no. 30, pp. 16465–16480, 2021.

[15] S. Bao, A. Ebadi, M. Toughani, J. Dalle, A. Maseleno, Baharuddin, and A. Yıldızbası, "A new method for optimal parameters identification of a PEMFC using an improved version of monarch butterfly optimization algorithm," *International Journal of Hydrogen Energy*, vol. 45, no. 35, pp. 17882–17892, 2020.

[16] R. Syah, L. A. Isola, J. W. G. Guerrero, W. Suksatan, D. Sunarsi, M. Elveny, A. F. Alkaim, L. Thangavelu, and S. Aravindhan, "Optimal parameters estimation of the PEMFC using a balanced version of water strider algorithm," *Energy Reports*, vol. 7, pp. 6876–6886, 2021.

[17] J. Luna, E. Usai, A. Husar, and M. Serra, "Nonlinear observation in fuel cell systems: A comparison between disturbance estimation and high-order sliding-mode techniques," *International Journal of Hydrogen Energy*, vol. 41, no. 43, pp. 19737–19748, 2016.

[18] Y. Zhu, J. Zou, S. Li, and C. Peng, "An adaptive sliding mode observer based near-optimal OER tracking control approach for PEMFC under dynamic operation condition," *International Journal of Hydrogen Energy*, vol. 47, no. 2, pp. 1157–1171, 2022.

[19] A. Dali, S. Abdelmalek, A. Bakdi, and M. Bettayeb, "A novel effective nonlinear state observer based robust nonlinear sliding mode controller for a 6 kw proton exchange membrane fuel cell voltage regulation," *Sustainable Energy Technologies and Assessments*, vol. 44, p. 100996, 2021.

[20] H. Deng, Y. Cui, W. Chen, D. Cao, and W. Hu, "Projection algorithm-based nonlinear observation of internal states in fuel delivery systems with gas diffusion," *Journal of Power Sources*, vol. 483, p. 229184, 2021.

[21] J. Luna, E. Usai, A. Husar, and M. Serra, "Observation of the electrochemically active surface area in a proton exchange membrane fuel cell," in *Proc. of IECON 2016 - 42nd Annual Conference of the IEEE Industrial Electronics Society*, (Florence, Italy), pp. 5483–5488, 2016.

[22] M. Arcak, H. Görgün, L. M. Pedersen, and S. Varigonda, "A nonlinear observer design for fuel cell hydrogen estimation," *IEEE Transactions on Control Systems Technology*, vol. 12, no. 1, 2004.

[23] D. Zhou, Y. Wu, F. Gao, E. Breaz, A. Ravey, and A. Miraoui, "Degradation prediction of PEM fuel cell stack based on multiphysical aging model with particle filter approach," *IEEE Transactions on Industry Applications*, vol. 53, no. 4, pp. 4041–4052, 2017.

[24] J. Kimotho, T. Meyer, and W. Sextro, "PEM fuel cell prognostics using particle filter with model parameter adaptation," in *Proc. 2014 International Conference on Prognostics and Health Management*, (Cheney, WA, USA), pp. 1–6, 2014.

[25] K. Song, Y. Wang, X. Hu, and J. Cao, "Online prediction of vehicular fuel cell residual lifetime based on adaptive extended Kalman filter," *Energies*, vol. 13, no. 23, p. 6244, 2020.

[26] D. Zhou, F. Gao, E. Breaz, A. Ravey, and A. Miraoui, "Degradation prediction of PEM fuel cell using a moving window based hybrid prognostic approach," *Energy*, vol. 138, pp. 1175–1186, 2017.

[27] A. Dicks and D. Rand, *Fuel Cell Systems Explained*. Hoboken, NJ, USA: Wiley, 3rd ed., 2018.

[28] J. T. Pukrushpan, H. Peng, and A. G. Stefanopoulou, "Control-Oriented Modeling and Analysis for Automotive Fuel Cell Systems ," *Journal of Dynamic Systems, Measurement, and Control*, vol. 126, no. 1, pp. 14–25, 2004.

[29] F. Barbir, *PEM Fuel Cells: Theory and Practice*. Elsevier Academic Press, 2005.

[30] N. Gordon, D. Salmond, and A. Smith, "Novel approach to nonlinear/non-Gaussian Bayesian state estimation," *IEE Proceedings-F*, vol. 140, no. 2, pp. 107–113, 1993.

[31] E. Bølviken, P. Acklam, N. Christophersen, and J. Størdal, "Monte Carlo filters for non-linear state estimation," *Automatica*, vol. 37, no. 2, pp. 177–183, 2001.

[32] E. A. Wan and R. Van Der Merwe, "The unscented Kalman filter for nonlinear estimation," in *Proc. of IEEE 2000 Adaptive Systems for Signal Processing, Communications, and Control Symposium*, (Lake Louise, AB, Canada), pp. 153–158, 2000.

[33] F. Gustaffson, "Particle filter theory and practice with positioning applications," *IEEE Aerospace and Electronic Systems Magazine*, vol. 25, no. 7, 2000.

[34] L. Liao and F. Köttig, "A hybrid framework combining data-driven and model-based methods for system remaining useful life prediction," *Applied Soft Computing*, vol. 44, pp. 191–199, 2016.

[35] G. Revach, N. Shlezinger, R. J. G. van Sloun, and Y. C. Eldar, "KalmanNet: Data-driven Kalman filtering," in *Proc. of the IEEE International Conference on Acoustics, Speech, and Signal Processing*, pp. 3905–3909, 2021.

[36] S. Billings and I. Leontaritis, "Parameter estimation techniques for nonlinear systems," in *6th IFAC Symposium on Identification and Systems Parameter Estimation*, (Washington D.C., U.S.A), p. 427–432., 1982.

[37] S. Billings and W. Voon, "Least-squares parameter estimation algorithms for non-linear systems," *International Journal of Systems Science*, vol. 15, no. 6, pp. 601–615, 1984.

[38] A. Husar, S. Strahl, and J. Riera, "Experimental characterization methodology for the identification of voltage losses of PEMFC: Applied to an open cathode stack," *International Journal of Hydrogen Energy*, vol. 37, pp. 7309–7315, 2012.

[39] J. Luna, A. Husar, and M. Serra, "Nonlinear distributed parameter observer design for fuel cell systems," *International Journal of Hydrogen Energy*, vol. 40, no. 34, pp. 11322–11332, 2015.